

Optical study on topological superconductor candidate Sr-doped Bi_2Se_3

Jialun Liu(刘佳伦), Chennan Wang(王晨南), Tong Lin(林桐), Liye Cao(曹立叶), Lei Wang(王蕾), Jiaji Li(李佳吉), Zhen Tao(陶镇), Nan Shen(申娜), Rina Wu(乌日娜), Aifang Fang(房爱芳), Nanlin Wang(王楠林), and Rongyan Chen(陈荣艳)

Citation: Chin. Phys. B, 2022, 31 (**11**): 117402. DOI: 10.1088/1674-1056/ac7a10

What follows is a list of articles you may be interested in

Negative tunnel magnetoresistance in a quantum dot induced by interplay of a Majorana fermion and thermal-driven ferromagnetic leads

Peng-Bin Niu(牛鹏斌), Bo-Xiang Cui(崔博翔), and Hong-Gang Luo(罗洪刚)

Chin. Phys. B, 2021, 30 (**9**): 097401. DOI: 10.1088/1674-1056/abf10b

Evidence for topological superconductivity: Topological edge states in Bi_2Te_3/FeTe heterostructure

Bin Guo(郭斌), Kai-Ge Shi(师凯歌), Hai-Lang Qin(秦海浪), Liang Zhou(周良), Wei-Qiang Chen(陈伟强), Fei Ye(叶飞), Jia-Wei Mei(梅佳伟), Hong-Tao He(何洪涛), Tian-Luo Pan(潘天洛), Gan Wang(王干)

Chin. Phys. B, 2020, 29 (**9**): 097403. DOI: 10.1088/1674-1056/abaf9c

Topological superconductivity in a Bi_2Te_3/$NbSe_2$ heterostructure: A review

Hao Zheng(郑浩), Jin-Feng Jia(贾金锋)

Chin. Phys. B, 2019, 28 (**6**): 067403. DOI: 10.1088/1674-1056/28/6/067403

In-plane optical spectral weight redistribution in the optimally doped $Ba_{0.6}K_{0.4}Fe_2As_2$ superconductor

Xu Bing (许兵), Dai Yao-Min (戴耀民), Xiao Hong (肖宏), R. P. S. M. Lobo, Qiu Xiang-Gang (邱祥冈)

Chin. Phys. B, 2014, 23 (**8**): 087401. DOI: 10.1088/1674-1056/23/8/087401

Evolution of the 251 cm^{-1} infrared phonon mode with temperature in $Ba_{0.6}K_{0.4}Fe_2As_2$

Dai Yao-Min(戴耀民), Xu Bing(许兵), Shen Bing(沈冰), Xiao Hong(肖宏), Lobo R. P. S. M, and Qiu Xiang-Gang(邱祥冈)

Chin. Phys. B, 2012, 21 (**7**): 077403. DOI: 10.1088/1674-1056/21/7/077403

Optical study on topological superconductor candidate Sr-doped Bi_2Se_3

Jialun Liu(刘佳伦)[1], Chennan Wang(王晨南)[2,†], Tong Lin(林桐)[2], Liye Cao(曹立叶)[1], Lei Wang(王蕾)[1], Jiaji Li(李佳吉)[1], Zhen Tao(陶镇)[1], Nan Shen(申娜)[1], Rina Wu(乌日娜)[1], Aifang Fang(房爱芳)[1], Nanlin Wang(王楠林)[2,3], and Rongyan Chen(陈荣艳)[1,‡]

[1] *Center for Advanced Quantum Studies and Department of Physics, Beijing Normal University, Beijing* 100875, *China*
[2] *International Center for Quantum Materials, School of Physics, Peking University, Beijing* 100871, *China*
[3] *Collaborative Innovation Center of Quantum Matter, Beijing* 100871, *China*

(Received 18 February 2022; revised manuscript received 14 June 2022; accepted manuscript online 18 June 2022)

Utilizing infrared spectroscopy, we study the charge dynamics of the topological superconductor candidate $Sr_xBi_2Se_3$. The frequency-dependent reflectivity $R(\omega)$ demonstrates metallic feature and the scattering rate of the free carriers decreases with temperature decreasing. The plasma edge shows a slight blue shift upon cooling, similar to the behavior of $Cu_xBi_2Se_3$. As the carrier concentration n obtained by Hall resistivity increases slightly with the decreasing temperature, the effective mass is proved to increase as well, which is in contrast with that of $Cu_xBi_2Se_3$. We also perform the ultrafast pump-probe study on the $Sr_{0.2}Bi_2Se_3$ compounds. Resembling its parent compound Bi_2Se_3, three distinct relaxation processes are found to contribute to the transient reflectivity. However, the deduced relaxation times are quite different. In addition, the electron-optical-phonon coupling constant is identified to be $\lambda = 0.88$.

Keywords: topological superconductor, infrared spectroscopy, ultrafast spectroscopy

PACS: 74.70.–b, 78.30.–j, 78.47.jg **DOI:** 10.1088/1674-1056/ac7a10

1. Introduction

In recent years, topological superconductors (TSCs) have attracted a great deal of attention due to their great significance in both fundamental research and potential application in quantum computing.[1–9] A TSC can have a full gapped superconducting bulk state together with a topologically protected gapless surface state. Majorana quasiparticles, which is crucial to the future fault-tolerant quantum computer, are believed to exist in the surface state of TSCs.[10] Up to date, searching for TSC materials is still an important task since there are only a few candidates discovered.

In 2010, Hor *et al.*[11] found that superconductivity could be realized in the layered topological insulator Bi_2Se_3 by Cu intercalation. The obtained $Cu_xBi_2Se_3$ was soon proposed to be a topological superconductor with a full gap and an odd-parity paring symmetry by theoretical calculation.[3,12] Experimentally, a zero-bias conductance peak expected for a topological superconductor was observed by point-contact spectroscopy, possibly due to Majarona fermions.[13] Although a scanning tunneling microscope measurement suggests that $Cu_xBi_2Se_3$ is a conventional s-wave superconductor,[14] further investigations demonstrate that it is more likely to be caused by an odd-parity superconductivity with a cylindrical Fermi surface.[15] More importantly, a twofold symmetry of the superconductivity is broadly identified by a large number of angle-resolved experiments in spite of its threefold symmetric lattice, which provides strong bulk evidence on the topological superconductivity.[16,17] Similar behaviors are revealed in the Sr[18–23] and Nb[3,24–26] doped Bi_2Se_3 as well, and this spontaneous rotational-symmetry breaking or nematicity was found to persist even above the superconducting transition temperature in $Sr_xBi_2Se_3$, inferring the underlying connection between nematicity and unconventional superconductivity.

So far, there are still a lot of controversial issues in understanding the superconductivity in $M_xBi_2Se_3$ (M = Cu, Sr, and Nb). Among them, $Cu_xBi_2Se_3$ is very sensitive to air and intrinsically inhomogeneous, so it has a rather low superconducting volume fraction ($\sim$ 56%).[27] In contrast, the $Sr_xBi_2Se_3$ compound exhibits excellent stability in air[28] and has a much larger shielding volume fraction ($\sim$ 91.5% at 0.5 K),[29] therefore it is more extensively studied. Additionally, although $Sr_xBi_2Se_3$ hosts the lowest carrier density ($\sim 10^{19}$ cm^{-3}), its superconducting phase transition temperature ($\sim$ 2.9 K)[28,30] is very close to that of $Cu_xBi_2Se_3$ ($\sim$ 3.8 K)[11] and $Nb_xBi_2Se_3$ ($\sim$ 3 K). In this paper, we use infrared spectroscopy and ultrafast pump-probe technique to study the optical responses of $Sr_xBi_2Se_3$ in both equilibrium and non-equilibrium state. We find a very slight blue shift of the plasma edge, which is associated with the simultaneous variation of the concentration and effective mass of the itinerate carriers. In addition, the electron-phonon coupling strength is yielded by our time resolved measurements.

[†]Current address: Laboratory for Muon Spin Spectroscopy, Paul Scherrer Institute, CH-5232 Villigen, Switzerland
[‡]Corresponding author. E-mail: rychen@bnu.edu.cn

© 2022 Chinese Physical Society and IOP Publishing Ltd

2. Experimental

Single crystals of $Sr_xBi_2Se_3$ for nominal concentrations $x = 0.20$ were synthesized by the flux method.[28] The obtained crystals were easily cleaved with a silvery shining mirror-like surface. The typical dimensions of the obtained single crystals are about $3 \times 2.5 \times 0.5$ mm^3, as shown in the inset of Fig. 1(a). The x-ray diffraction (XRD) measurements were conducted along the basal plane and the results are shown in Fig. 1(a), which indicate the samples are of high purity and the surface is along the (00l) plane.

The temperature-dependent resistivity $\rho(T)$ and magnetization M were measured in a Quantum Design physical property measurement system (PPMS), as shown in Figs. 1(b) and 1(c). The resistivity $\rho(T)$ decreases with temperature decreasing in the normal state. It begins to drop dramatically at around 2.85 K and approaches zero at around 2.6 K, remarking the superconducting phase transition. A diamagnetic signal was observed in the magnetic susceptibility at the same time. The large residual resistivity value of ~ 110 and the narrow superconducting transition width both indicate the high quality of our single crystalline samples. Hall effect measurements were also performed in the PPMS with the temperature ranging from 300 K to 2 K in perpendicular magnetic fields up to ± 9 T. In the case that the orientation of the Hall electrode is not applied strictly perpendicular to the direction of the current in the basal plane of $Sr_{0.2}Bi_2Se_3$ single crystals, the Hall resistivity is defined as $\rho_{xy} = [\rho_{xy}(+B) - \rho_{xy}(-B)]/2$, where $\rho_{xy}(+B)$ and $\rho_{xy}(-B)$ are the Hall resistance measured by increasing and decreasing the magnetic fields, respectively.

Infrared spectroscopic studies were performed on the as-grown shinny surfaces of $Sr_{0.2}Bi_2Se_3$ single crystals with a Bruker IFS 80V in the frequency range from 30 to 25000 cm^{-1} and as a function of temperature. In the measurement of frequency-dependent reflectivity $R(\omega)$, either gold or aluminum coating techniques are adopted in order to eliminate the impact of microscopic surface textures of the single crystalline compound. The real part of the optical conductivity $\sigma_1(\omega)$ is derived through the Kramers–Kronig transformation of the reflectivity $R(\omega)$, which is extrapolated by a Hagen–Rubens relation to zero at the low frequency end, and x-ray scattering functions[31] for the high energy extrapolations.

Ultrafast optical pump-probe spectroscopy of $Sr_{0.2}Bi_2Se_3$ was performed between 4 and 150 K. In this study, we used a femtosecond Ti:sapphire amplifier as the light source for probe beam, which can produce an 800 nm pulsed laser at 1 kHz repetition. The pump beam with a wavelength of 400 nm is obtained through the ultraviolet frequency doubling BBO crystal. The 100 fs time duration of the laser pulses enables ultrashort time-resolved measurement. The pump intensity was set to be ~ 2 μJ/cm^2 and the probe intensity was 10 times lower.

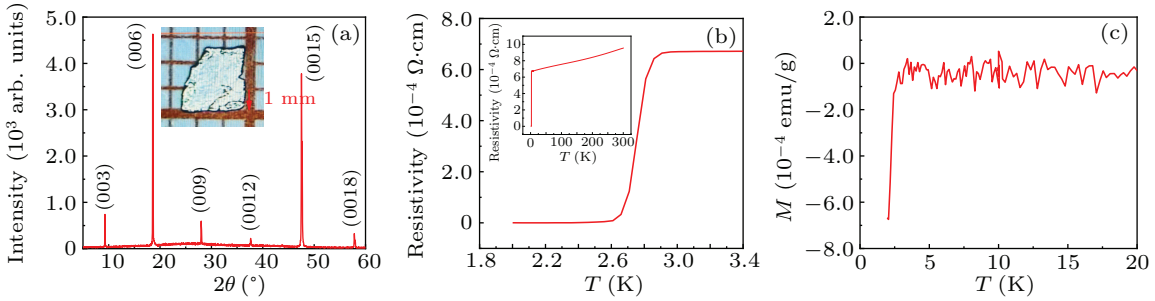


Fig. 1. (a) XRD pattern of $Sr_{0.2}Bi_2Se_3$ single crystal. The inset is a photo of the single crystal. (b) The resistivity $\rho(T)$ as a function of temperature in the range of 1.8–3.4 K. The inset shows the resistivity $\rho(T)$ as a function of temperature in the 0–300 K range. (c) Magnetization M as a function of temperature in the 0–20 K range.

3. Results and discussion

The frequency-dependent reflectivity $R(\omega)$ is displayed in Fig. 2(a). It can be seen that $R(\omega)$ approaches unit at low frequencies and increases with decreasing temperature in the far infrared region, showing a typical metallic response. As the frequency increases, $R(\omega)$ drops rapidly and reaches a minimum around 790 cm^{-1} at 300 K, which is usually called a "screened" plasma edge. The sharpness of the plasma edge indicates a good metallic property while the small edge minimum corresponds to a low carrier density. According to a previous report,[32] the reflectivity of Bi_2Se_3 and $Cu_xBi_2Se_3$ displays plasma edges as well. Their edge minima locate at around 550 cm^{-1} and 1150 cm^{-1}, respectively. The intermediate value for $Sr_{0.2}Bi_2Se_3$ obtained in our measurements demonstrates that the Sr intercalation has indeed introduced free carriers into the parent compound Bi_2Se_3, but not as much as Cu doping.

As shown in Fig. 2(b), the real part of the optical conductivity σ_1 shows a Drude component at the low energy range, reflecting the metallic nature of $Sr_{0.2}Bi_2Se_3$. The zero-frequency conductivity increases upon cooling, consistent with the behavior of the resistivity $\rho(T)$. Moreover, the Drude component becomes more sharp as temperature decreases, indicating the reduction of the scattering rate of free carriers. To qualitatively study the evolution of the physical properties, we decompose the real part of the optical conduc-

tivity σ_1 according to the Drude–Lorentz model:

$$\sigma_1(\omega) = \frac{\omega_p^2}{4\pi}\frac{\gamma_D}{\omega^2+\gamma_D^2} + \sum_j \frac{S_j^2}{4\pi}\frac{\gamma_j\omega^2}{(\omega_j^2-\omega^2)^2+\omega^2\gamma_j^2}, \quad (1)$$

where ω_p and γ_D are the plasma frequency and scattering rate of the itinerate carriers, while ω_j, γ_j and S_j are the resonant frequency, damping and strength of the jth Lorentz oscillators, respectively. The first term on the right-hand side of Eq. (1) is the Drude component modeling intraband transitions of free electrons while the second Lorentz term describes interband transitions across energy gaps.

A representative example of the fitting results of $\sigma_1(\omega)$ at 10 K is plotted in the inset of Fig. 2(b), where one Durde and four Lorentz terms are employed. The four interband transitions, centered at 5300 cm^{-1}, 8000 cm^{-1}, 12640 cm^{-1}, and 23920 cm^{-1}, are basically temperature independent. It is worth noting that these four Lorentz peaks located very closely to that of $Cu_xBi_2Se_3$, which suggests that the band structure of the parent compound Bi_2Se_3 is quite stable against doping, providing a solid platform to realize topological superconductivity.

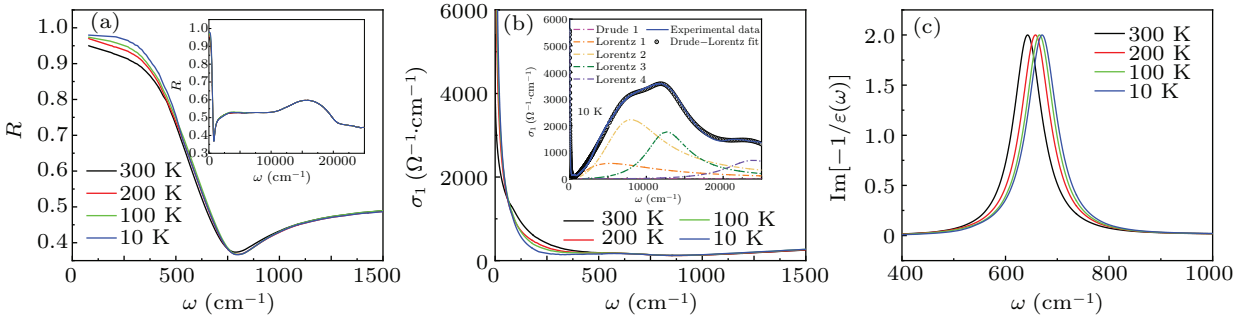


Fig. 2. (a) Reflectivity of $Sr_{0.2}Bi_2Se_3$ single crystals in the frequency range of 0–1500 cm^{-1} at different temperatures. The inset shows the reflectivity in the frequency range of 0–25000 cm^{-1}. (b) The real part of the optical conductivity σ_1 and (c) the energy loss function $\mathrm{Im}[-1/\varepsilon(\omega)]$ of the $Sr_{0.2}Bi_2Se_3$ single crystal. The inset of (b) shows the real part of the optical conductivity σ_1 in the frequency range of 0–25000 cm^{-1} at different temperatures.

Among the fitting parameters, the plasma frequency ω_p is related to the itinerate carrier density n and effective mass m^* by $\omega_p^2 = 4\pi ne^2/m^*$. A value of 1674 cm^{-1} was obtained by our Drude–Lorentz fitting, which is almost temperature independent within the error margin. Note that this value is an order of magnitude smaller than most of the conventional metals, indicating a much lower carrier density. In order to capture the variation of the plasma frequency with temperature more precisely, we calculate the frequency-dependent energy loss function $\mathrm{Im}[-1/\varepsilon(\omega)]$, as shown in Fig. 2(c). The peak position of the energy loss function can reflect the screened plasma frequency $\omega_p' = \omega_p/\sqrt{\varepsilon_\infty}$, which shifts from 640 cm^{-1} at 300 K to 670 cm^{-1} at 10 K.

Shifts of plasma frequency were also observed in the Bi_2Se_3 and $Cu_xBi_2Se_3$ materials. Bi_2Se_3 shows a red shift and $Cu_xBi_2Se_3$ exhibits a blue shift with temperature decreasing. The redshift of Bi_2Se_3 was ascribed to the decreasing carrier density, which is caused by the reduction of thermal excitations. However, Hall experiments reveal that the carrier density of $Cu_xBi_2Se_3$ remains unchanged with temperature decreasing,[8] so Tao and coauthors attributed its blueshift to the reduction of effective mass, induced by the shift of Fermi level relative to the band structure. In order to verify whether the blueshift of $Sr_xBi_2Se_3$ shares a similar underling mechanism with $Cu_xBi_2Se_3$, we performed the Hall resistivity measurement on $Sr_xBi_2Se_3$.

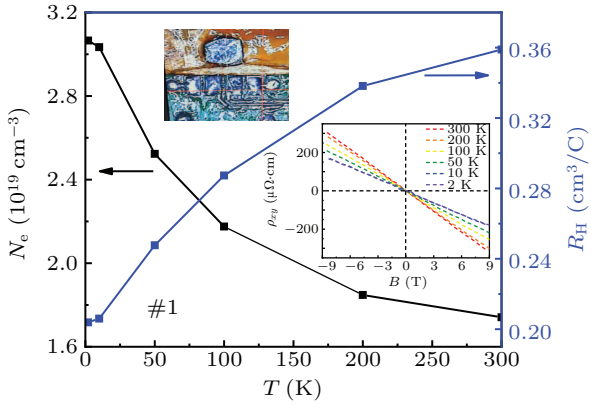


Fig. 3. The carrier concentration and Hall coefficient versus temperature. The upper inset is a photograph of the sample and the lower inset shows its Hall resistivity versus applied magnetic field at different temperatures.

As plotted in the inset of Fig. 3, the Hall resistivity is proportional to the applied magnetic field B in the range from -9 T to 9 T at all selective temperatures. The negative slope indicates that electrons are the only type of dominated carriers. As temperature decreases, the Hall coefficient R_H decreases monotonically. According to $R_H = -1/ne$, the carrier concentration n increases from 1.74×10^{19} cm^{-3} at 300 K to 3.07×10^{19} cm^{-3} at 2 K. It is well known that the chemical potential is related to temperature by $\mu(T) = E_F[1-\frac{\pi^2}{12}(\frac{k_BT}{E_F})^2]$, where E_F is the Fermi energy and k_B is the Boltzmann constant. When E_F is relatively low, which works for $Sr_xBi_2Se_3$ due to its small carrier density, the increase of temperature could lead to a downward shift of the chemical potential. Since

the carriers are mainly electrons, the lowering of chemical potential at higher temperatures may give rise to a reduction of the carrier density.

Now that we know the values of carrier concentration n and the screened plasma frequency ω_p', the evolution of effective mass m^* with temperature could be obtained. The ratio of m^* from 300 K to 10 K is estimated to be about 0.625, which indicates an increase of m^* upon cooling. By comparison, the effective mass of $Cu_xBi_2Se_3$ was reported to decrease from $m^* = 0.4215m_e$ at 300 K to $m^* = 0.3888m_e$ at 10 K, which was ascribed to the change of dispersion near E_F. Adopting a plasma frequency $\omega_p = 1674$ cm^{-1} and a carrier density $n = 3.03 \times 10^{19}$ cm^{-3}, the effective mass of $Sr_{0.2}Bi_2Se_3$ at 10 K is calculated to be $0.970m_e$, which is much larger than the value of $Cu_xBi_2Se_3$. As the carrier density of $Sr_{0.2}Bi_2Se_3$ is very close to that of Bi_2Se_3 and much smaller than that of $Cu_xBi_2Se_3$, the Fermi level of $Sr_xBi_2Se_3$ is supposed to be much closer to that of Bi_2Se_3. Especially, the effective mass of $Sr_{0.2}Bi_2Se_3$ nearly approached the static electron mass m_e at 4 K, suggesting that the Fermi level locates near a parabolic band. Considering that there are multiple conduction and valence bands near the Fermi level located at different momentum positions in the Brillouin zone, there may be a thermal redistribution between bands with different effective masses, as proposed by Park *et al.*[33] The differences between $Sr_xBi_2Se_3$ and $Cu_xBi_2Se_3$ reveal the complexity of the band structure near the Fermi level.

In order to get more information about the bulk band structure of $Sr_{0.2}Bi_2Se_3$, we also performed ultrafast pump-probe measurements. Figure 4(a) shows the photoinduced reflectivity $\Delta R/R$ in long (main panel) and short (inset) timescales at room temperature. Its overall profile highly resembles that of the parent compound Bi_2Se_3.[34,35] First of all, two strong oscillations could be resolved. The slow one with a frequency lower than 0.1 THz is almost temperature independent and most likely resulted from the coherent longitudinal acoustic phonons. The second fast oscillation located at $\omega_{fast} = 2.17$ THz at room temperature, which is slightly higher than that observed in Bi_2Se_3 (2.15 THz), inferring the structure modulation caused by the Sr intercalation. Furthermore, a very gentle softening of ω_{fast} with temperature increasing is illustrated in Fig. 4(c), owing to the thermal effect.

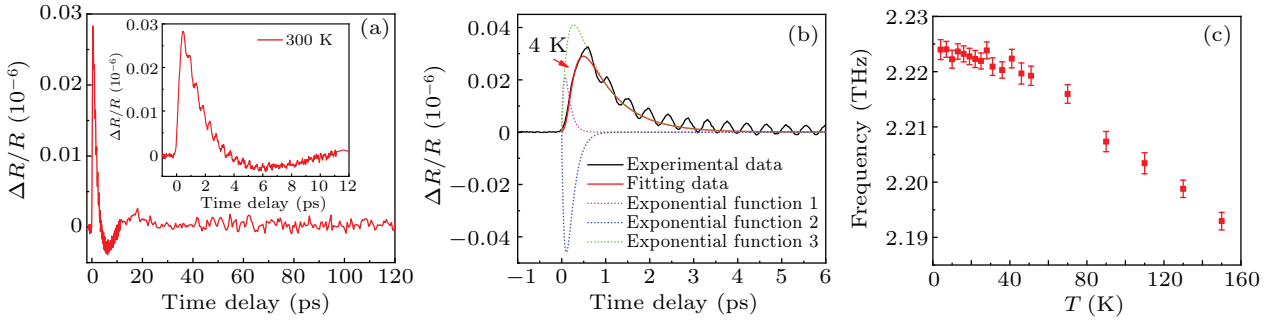


Fig. 4. (a) The transient reflectivity $\Delta R/R$ of $Sr_{0.2}Bi_2Se_3$ at room temperature over long (main panel) and short (inset) timescales. (b) The fitting results of $\Delta R/R$ at 4 K. The black and red solid line represent the experimental and fitting data, respectively. The three dotted lines are the three exponential functions used for fitting. The red arrow marks the kink shown in the rising edge. (c) The frequency of the fast oscillation as a function of temperature.

The transient reflectivity $\Delta R/R$ displays a sharp rise persisting until 0.5 ps, which is much longer than most conventional semiconductors and metals ($\sim$ 300 fs).[36] According to the two-temperature model, this process is usually governed by the thermalization of carriers through electron–electron interactions.[37,38] Especially, a kink can be resolved at around 0.3 ps, indicating more than one relaxation channels. Following the procedure used to deal with the parent compound,[34] we find that the non-oscillating part of our data can be well reproduced by three-exponential decay as well. The fitting results at 4 K are shown in Fig. 4(b).

Similar to Bi_2Se_3, one negative amplitude A_2 and two positive amplitudes A_1 and A_3 are yielded by fitting. The first (third) relaxation channel is assigned to be governed by the couplings between the excited quasiparticles and optical (acoustic) phonon modes in Bi_2Se_3, whereas the second one is suggested to be related to the defect-induced charge trapping.[34] Here, we believe these three channels work for $Sr_{0.2}Bi_2Se_3$ as well, due to their remarkable similarity. However, the corresponding relaxation times of $Sr_{0.2}Bi_2Se_3$ are identified to be $\tau_1 = 0.095 \pm 0.01$ ps, $\tau_2 = 0.15 \pm 0.02$ ps, and $\tau_3 = 0.80 \pm 0.05$ ps, which are quite different from the values for the parent compound ($\tau_1 = 0.11 \pm 0.02$ ps, $\tau_2 = 0.32 \pm 0.03$ ps, and $\tau_3 = 2.3 \pm 0.2$ ps). It is worth remarking that the fitting values of the parameters depend partly on the choices of initial values, and the above results are the best outcome we could obtain.

In time-resolved ultrafast spectroscopy, it is well known that the thermal relaxation rate ($\gamma_T = 1/\tau$) for the excited quasiparticles returning back to local equilibrium state via electron-phonon interaction satisfies $\gamma_T = 3\hbar\lambda\langle\Omega^2\rangle\pi k_B T$,[38,39] where λ is the electron–phonon coupling constant, and Ω is the phonon frequency, and k_B is the Boltzmann constant, and T_e is the electron temperature

after photo-excitation. Since the relaxation times τ_1 and τ_3 are mainly determined by the electron-phonon coupling process, their smaller values compared to the parent compound indicate that both the electron–optical-phonon coupling and electron–acoustic-phonon coupling are enhanced by the Sr doping, which agrees well with the results of Raman measurements.[40] At the same time, Sr doping will introduce more defects into the system, which may probably lead to decrease of τ_2.

Since the fast oscillation observed in our measurement is very close to the optical A_{1g} mode,[40–42] we can obtain the electron-optical phonon coupling constant by adopting Ω_1 = 2.22 THz at 4 K. The quasiparticle temperature T_e could be calculated by

$$T_e = \left\langle \sqrt{T_L^2 + \frac{2(1-R)F}{k_\nu l_s} e^{\frac{-z}{l_s}}} \right\rangle, \tag{2}$$

where $R = 0.56$ according to our infrared spectroscopy results; $k_\nu = k\rho_n$ represents the specific heat capacity coefficient per unit volume with $k = 0.1$ mJ/mol/K^2[17] being the heat capacity coefficient and ρ_n the mole density; $l_s = 2.3$ μm[43] is the penetration depth; and z is the distance from the sample surface. We obtain $T_e = 118.3$ K with $T_L = 4$ K, using the lattice constant $a = 4.1369$ Å and $c = 28.598$ Å.[28] With the above values of T_e and $\tau_1 = 0.095$ ps, we can derive $\lambda_1 \langle \Omega_1^2 \rangle = 1.71 \times 10^{26}$ Hz^2 and the electron–phonon coupling constant $\lambda_1 = 0.88$, which could be useful in determining the underlying superconducting mechanism.

4. Conclusion

In summary, we have performed infrared spectroscopy and ultrafast time-resolved optical spectroscopy on the topological superconductor candidate $Sr_{0.2}Bi_2Se_3$. The equilibrium optical response of $Sr_{0.2}Bi_2Se_3$ is characterized by a slight blue shift of the plasma frequency with temperature decreasing. As the carrier density is demonstrated to increase upon cooling by Hall measurements, the effective mass is proved to show a similar trend, which is different from the behavior of $Cu_xBi_2Se_3$. Since the Fermi level of $Sr_{0.2}Bi_2Se_3$ is lower than that of $Cu_xBi_2Se_3$ and closer to the conduction band minimum, we believe this difference is caused by the complex band structure near the Fermi level. Our non-equilibrium measurements reveal three relaxation channels in $Sr_xBi_2Se_3$, similar to the spectra of its parent compound Bi_2Se_3. However, the relaxation times are quite different due to the change of electron-phonon coupling strength and introduction of defected by Sr doping. We also obtain the electron-optical-phonon coupling constant $\lambda = 0.88$.

Acknowledgements

Project supported by the National Natural Science Foundation of China (Grant Nos. 12074042 and 11704033), the National Key Research and Development Program of China (Grant Nos. 2021YFA1400400 and 2016YFA0302300), and the Fundamental Research Funds for the Central Universities.

References

[1] Qi X L, Hughes T L, Raghu S and Zhang S C 2009 *Phys. Rev. Lett.* **102** 187001
[2] Wray L A, Xu S Y, Xia Y Q, Hor Y S, Qian D, Fedorov A V, Lin H, Bansil A, Cava R J and Hasan M Z 2010 *Nat. Phys.* **6** 855
[3] Fu L and Berg E 2010 *Phys. Rev. Lett.* **105** 097001
[4] Sato M and Ando Y 2017 *Rep. Prog. Phys.* **80** 076501
[5] Fu L and Kane C L 2007 *Phys. Rev. B* **76** 045302
[6] Fu L and Kane C L 2008 *Phys. Rev. Lett.* **100** 096407
[7] Neupane M, Ishida Y, Sankar R, Zhu J X, Sanchez D S, Belopolski I, Xu S Y, Alidoust N, Hosen M M, Shin S, Chou F C, Hasan M Z and Durakiewicz T 2016 *Sci. Rep.* **6** 22557
[8] Kriener M, Segawa K, Ren Z, Sasaki S and Ando Y 2011 *Phys. Rev. Lett.* **106** 127004
[9] Yonezawa S 2016 *AAPPS Bull.* **26** 3
[10] Ando Y and Fu L 2015 *Annu. Rev. Condens. Matter Phys.* **6** 361
[11] Hor Y S and Williams A J, Checkelsky J G, Roushan P, Seo J, Xu Q, Zandbergen H W, Yazdani A, Ong N P and Cava R J 2010 *Phys. Rev. Lett.* **104** 057001
[12] Fu L 2014 *Phys. Rev. B* **90** 100509(R)
[13] Sasaki S, Kriener M, Segawa K, Yada K, Tanaka Y, Sato M and Ando Y 2011 *Phys. Rev. Lett.* **107** 217001
[14] Levy N, Zhang T, Ha J, Sharifi F, Talin A A, Kuk Y and Stroscio J A 2013 *Phys. Rev. Lett.* **110** 117001
[15] Mizushima T, Yamakage A, Sato M and Tanaka Y 2014 *Phys. Rev. B* **90** 184516
[16] Hashimoto T, Yada K, Yamakage A, Sato M and Tanaka Y 2013 *J. Phys. Soc. Jpn.* **82** 044704
[17] Yonezawa S, Tajiri K, Nakata S, Nagai Y, Wang Z W, Segawa K, Ando Y and Maeno M 2017 *Nat. Phys.* **13** 123
[18] Du G, Li Y F, Schneeloch J, Zhong R D, Gu G D, Yang H, Lin H and Wen H H 2017 *Sci. China Phys. Mech. Astron.* **60** 037411
[19] Pan Y, Nikitin A M, Araizi G K, Huang Y K, Matsushita Y, Naka T and Visser A 2016 *Sci. Rep.* **6** 28632
[20] Nikitin A M, Pan Y, Huang Y K, Naka T and Visser A 2016 *Phys. Rev. B* **94** 144516
[21] Smylie M P, Willa K, Claus H, Koshelev A K, Song K W, Kwok W K, Islam Z, Gu G D, Schneeloch J A, Zhong R D and Welp U 2018 *Sci. Rep.* **8** 7666
[22] Willa K, Willa R, Song K W, Gu G D, Schneeloch J A, Zhong R D, Koshelev A E, Kwok W K and Welp U 2018 *Phys. Rev. B* **98** 184509
[23] Kostylev I, Yonezawa S, Wang Z W, Ando Y and Maeno Y 2020 *Nat. Commun.* **11** 4152
[24] Shen J Y, He W Y, Yuan N, Huang Z, Cho C W, Lee S H, Hor Y S, Law K T and Lortz R 2017 *npj Quantum Mater.* **2** 59
[25] Asaba T, Lawson B J, Tinsman C, Chen L, Corbae P, Li G, Qiu Y, Hor Y S, Fu L and Li L 2017 *Phys. Rev. X* **7** 011009
[26] Cho C W, Shen J Y, Lyu J, Atanov O, Chen Q X, Lee S H, Hor Y S, Gawryluk D J, Pomjakushina E, Bartkowiak M, Hecker M, Schmalian J and Lortz R 2020 *Nat. Commun.* **11** 3056
[27] Schneeloch J A, Zhong R D, Xu Z J, Gu G D and Tranquada J M 2015 *Phys. Rev. B* **91** 144506
[28] Liu Z H, Yao X, Shao J F, Zuo M, Pi L, Tan S, Zhang C J and Zhang Y H 2015 *J. Am. Chem. Soc.* **137** 10512
[29] Kobayashi K, Ueno T, Fujiwara H, Yokoya T and Akimitsu J 2017 *Phys. Rev. B* **95** 180503(R)
[30] Shruti, Maurya V K, Neha P, Srivastava p and Patnaik S 2015 *Phys. Rev. B* **92** 020506(R)
[31] Tanner D B 2015 *Phys. Rev. B* **91** 035123
[32] Dong T, Yuan R H, Shi Y G and Wang N L 2013 *Chin. Phys. Lett.* **30** 127801

[33] Park H J, Sandilands L J, You J S, Ji H S, Sohn C H, Han J W, Moon S J, Kim K W, Shim J H, Kim J S and Noh T W 2016 *Phys. Rev. B* **93** 205122

[34] Qi J, Chen X, Yu X, Zimansky P C, Smirnov D, Tolk N H, Miotkowski I, Cao H, Chen Y P,Wu Y, Qiao S and Jiang Z 2010 *Appl. Phys. Lett.* **97** 182102

[35] Glinka Y D, Babakiray S, Johnson T A, Bristow A D, Holcomb M B and Lederman D 2013 *Appl. Phys. Lett.* **103** 151903

[36] Rast S, Schneider M L, Onellion M, Zeng X H, Si W D, Xi X X, Abrecht M, Ariosa D, Pavuna D, Ren Y H, Lüpke G and Perakis I 2001 *Phys. Rev. B* **64** 214505

[37] Kaganov M I, Lifshitz E M and Tanatarov L V 1957 *Sov. Phys. JETP* **4** 173

[38] Allen P B 1987 *Phys. Rev. Lett.* **59** 1460

[39] Wu Q, Zhou H X, Wu Y L, Hu L L, Ni S L, Tian Y C, Sun F, Zhou F, Dong X L, Zhao Z X and Zhao J M 2020 *Chin. Phys. Lett.* **37** 097802

[40] Li M T, Fang Y F, Pei C Y, Qi Y P and Wang L 2020 *J. Phys.: Condens. Matter* **32** 385701

[41] Richter W and Becker C R 1977 *Phys. Status Solidi B* **84** 619

[42] Sohier T, Ponomarev E, Gibertini M, Berger H, Marzari N, Ubrig N and Morpurgo A F 2019 *Phys. Rev. X* **9** 031019

[43] Leng H, Cherian D, Huang Y K, Orain J C, Amato A and Visser A 2018 *Phys. Rev. B* **97** 054503